Coupled non-equilibrium fluctuations in a polymeric ternary mixture

L. García-Fernández, P. Fruton, Henri Bataller, J. M Ortiz de Zárate, Fabrizio Croccolo

Coupled non-equilibrium fluctuations in a polymeric ternary mixture

L. García-Fernández[1,2], P. Fruton[1], H. Bataller[1], J.M. Ortiz de Zárate[3] and F. Croccolo[1]

[1]*Laboratoire des Fluides Complexes et leurs Réservoirs – IPRA, UMR5150, E2S-Univ Pau & Pays Adour/CNRS/Total, 1 Allée du Parc Montaury,64600, Anglet, France.*

[2]*Centre National d´Études Spatiales (CNES),2, Place Maurice Quentin, 75001 Paris, France.*

[3]*Departamento de Estructura de la Materia, Física Térmica y Electrónica, Facultad de Ciencias Físicas, Universidad Complutense de Madrid. Plaza de las Ciencias 1, 28040 Madrid, Spain.*

Abstract

We investigate by dynamic shadowgraphy the non-equilibrium fluctuations at the steady state of a thermodiffusion experiment in a polymeric ternary mixture of polystyrene-toluene-n-hexane. The structure function of the refractive index reveals the existence of quite different decay times, thus requiring the analysis of a wide range of correlation times. This is related to the simultaneous presence of three distinct decay modes corresponding to (from fastest to slowest) relaxation of temperature fluctuations, of the concentration fluctuations of the mixed solvent, and of the concentration fluctuations of the polymer in the binary solvent. An investigation of the decay times at the corresponding diffusive regimes provides a measurement of the thermal diffusivity and the two eigenvalues of the mass diffusion matrix of the ternary mixture. Similar experiments were performed in the past but here, to suppress the confinement effect and obtain a more direct comparison with the theory, a thicker sample is studied. Moreover, also a faster camera is used allowing the experimental observation of faster modes, like the propagative ones. The experimental values of the decay times are eventually compared with those predicted by different available theories. Finally, we present a more complete theoretical model to describe the non-equilibrium fluctuations in the bulk of a ternary mixture at the steady state of a thermodiffusion experiment.

Keywords: Multicomponent mixtures, Polymer, Thermodiffusion, Shadowgraphy, Non-equilibrium, Fluctuations

1. Introduction

The majority of the fluids encountered in nature and industry are multicomponent mixtures. The knowledge of their transport properties is crucial for many different applications from both scientific and technological points of view. The efficiency of exploitation of the crude oil wells, as well as the environmental alternative focused on the CO_2 storage in deep brine aquifers, are some recent examples showing the interest of studying the transport properties of multicomponent mixtures subjected to non-equilibrium conditions [1, 2]. Complex fluids in non-equilibrium conditions exhibit giant fluctuations of the thermodynamic variables, the so-called non-equilibrium fluctuations (NEFs) [3-5]. By analysing NEFs through light scattering techniques, the transport properties of the fluid can be determined both at atmospheric [6] and at high pressure [7].

The non-equilibrium condition can be induced, for example, by applying a temperature gradient to a multicomponent fluid mixture, thus inducing a composition gradient within the fluid by means of the thermodiffusion, or Soret effect [8-10]. This transport process can be investigated by optical techniques and particularly by light scattering thanks to its ability to visualize NEFs without altering the intrinsic properties of the fluid. In this work, dynamic shadowgraphy has been adopted [11-13] to study the fluctuations of the refractive index as generated by the NEFs of the thermodynamic variables, like temperature and concentrations. By shadowgraphy, a large range of fluctuations sizes λ or, conversely, wave numbers $q = 2\pi/\lambda$, can be investigated at the same time. This approach, combined with statistical analysis, represents a powerful characterization technique able to provide simultaneous reliable measurements of different

transport properties, like mass diffusion coefficient or thermal diffusivity as well as Soret coefficient [6, 14, 15].

A suitable characterization of transport processes in complex mixtures requires a deep understanding of simpler fluids. So far, only binary mixtures [10, 16] have been extensively characterized. The extension of theories and experiments from binary to ternary mixtures requires further development due to the intrinsic and significant increase of difficulty with the number of components of the mixture. Currently, a great effort is devoted to investigate the transport phenomena in ternary mixtures, as performed in the present study. Thermodiffusion experiments in ternary mixtures are performed on ground, by using different optical techniques [10, 14, 17, 18], or in microgravity in order to avoid both convection and sedimentation. The thermodynamic characterization of ternary mixtures is one of the objectives of the following ESA projects: Diffusion Coefficient Measurements in ternary mIXtures (DCMIX) [18-23], Soret Coefficients in Crude Oil (SCCO) [1, 24-27] and Giant Fluctuations [28], as further elaborated in a recent colloquium paper [29].

As a benchmark ternary mixture, the tetraline, isobutylbenzene and n-dodecane sample has been studied by digital interferometry on ground and in microgravity within the DCMIX experiments [18, 19, 30-38]. In addition, Bataller et al. [17] investigated this mixture on ground by one-wavelength shadowgraphy. Since no other alternative was available at that time, Bataller et al. [17] compared their experimental results with the theory of concentration NEFs developed for ternary mixtures in the absence of gravity [39]. The two concentration modes related to the presence of the two independent components could not be distinguished experimentally, and only an average of the two eigenvalues of the mass diffusion matrix could be provided. This result is expected, as the mixture is composed of similar-size molecules, and consequently the two eigenvalues of the diffusion coefficient matrix are very similar to each other. The two eigenvalues $\widehat{D}_1$ and $\widehat{D}_2$ of the diffusion matrix **D** need to be different enough to distinguish the

two concentration modes. An equivalent way to set this statement is to define a dimensionless number $Dr = \widehat{D}_2/\widehat{D}_1$ (Dr for Diffusion eigenvalue Ratio and $\widehat{D}_1$ representing the slowest diffusion mode) and require it to satisfy the relation $Dr \gg 1$. A ternary mixture containing a polymer dissolved in a binary mixed solvent is a good candidate for such measurement, due to the very different molecular size of its components and, correspondingly, a value of $Dr \approx 10$. This was experimentally proved for the diluted polymeric ternary mixture of polystyrene-toluene-n-hexane, as reported in [14], where a layer of $L = 2\,mm$ thick was investigated by using one-wavelength shadowgraphy at a single image acquisition frequency of 28 Hz. By adopting the theoretical model of ternary mixtures in the absence of gravity, the dynamics of the NEFs could be analysed for large wave numbers [14]. From such analysis, it was only possible to determine the two eigenvalues of the mass diffusion matrix and the thermal diffusivity. Afterwards, the diffusion matrix was simplified by neglecting the off-diagonal elements and the result was utilised for obtaining an analytical relationship between the two Soret coefficients, without an independent measurement of them. More recently [40], we have further developed the theory of NEFs to include the effect of gravity, but not confinement so that a direct comparison with the data of Ref. [14] is impossible since fluid layer thickness of only 2 mm makes confinement effects important, as evidenced in related literature for binary mixtures [41, 42].

In the present study, we perform a new shadowgraph experiment on a similar ternary mixture, but in this case a thicker sample with vertical extension of $L = 5\,mm$ is analysed in order to avoid the confinement effect, and be able to compare the experimental results with the theory of NEFs including gravity [40]. The present measurements are also carried out with a faster camera, allowing a more accurate characterization of thermal fluctuations and, thus, a better separation of them from concentration ones. Additionally, a new procedure of image acquisition combined with the concatenation of the structure functions allows us to investigate a wider

range of correlation times, as required for a complete analysis of this mixture that has a wide range of decay times. The experimental results are thus compared for the first time with the theoretical model developed for ternary mixtures in the presence of gravity [40], as well as with the recently developed theory that includes the coupling of velocity, thermal and solutal NEFs in the case of binary mixtures [43]. These comparisons suggest that a further development of the theory is required, in particular to include the coupling between the different NEFs in the case of the ternary mixture. As part of the contents of this paper we present such a development and compare with the experimental data.

2. Experimental procedure

2.1 Polymeric solution preparation and characterization

The sample is prepared by dissolving 2 wt% of polystyrene (PS, $M_\omega = 4730\ g/mol$, DIN-Poly(styrene) 4730 DA – PDI 1.03 by PSS-polymer) in 49 wt% toluene (Sigma-Aldrich, 24,451-1, 99.8%) and 49 wt% n-hexane (Sigma-Aldrich, 13,938-6, >99%) at ambient temperature by using a magnetic stirrer. The thermophysical properties of the mixture, such as density, viscosity and both thermal and mass expansion coefficients are determined.

The kinematic viscosity ν is measured at 25ºC by a capillary viscometer (Ubbelohde SCHOTT). The thermal and mass expansion coefficients, α and β_i, respectively, are defined as follows:

$$\alpha = -\frac{1}{\rho}\left(\frac{\partial \rho}{\partial T}\right)_{\omega,p}, \tag{1}$$

$$\beta_i = \frac{1}{\rho}\left(\frac{\partial \rho}{\partial \omega_i}\right)_{T,p}, \tag{2}$$

where ρ is the mixture density, T is the temperature and ω_i is the concentration of component i in mass fraction. Following a common notation, components are ordered according to their

125 (pure) density, hence, in this study 1 corresponds to PS, 2 corresponds to toluene and 3
126 corresponds to n-hexane.
127 The coefficients α and β_i are indirectly determined from measurements of the mixture density
128 performed at different conditions through a Density Meter (ANTON PAAR, DMA 5000). For
129 the thermal expansion coefficient, the density is measured at different temperatures (from 23 to
130 27°C), while keeping the concentrations constant at $\omega_1 = 0.02$ and $\omega_2 = 0.49$. The mass
131 expansion coefficients are obtained after measuring the density at different concentrations while
132 keeping the temperature constant at 25°C. To obtain the mass expansion coefficient of the
133 polymer in the mixed solvent, β_1, the concentration of the polystyrene is changed from $\omega_1 =$
134 0.000 to $\omega_1 = 0.035$, keeping $\omega_2 = \omega_3$. For the mass expansion coefficient of the mixed
135 solvent, β_2, the composition of the mixed solvent is modified from $\omega_2 = 0.47$ to $\omega_2 = 0.51$,
136 keeping $\omega_1 = 0.02$ constant. Measured values of ρ, ν, α and β_i are summarized in Table 1. The
137 values of ρ, ν, α and β_2 are consistent with those reported in [44], determined for the equi-
138 massic toluene-n-hexane binary mixture at $T_{mean} = 25\ °C$. The measurements of viscosity and
139 density are repeated at least three times for each sample. The values reported in Table 1 are
140 calculated as the average of the three measurements and the corresponding uncertainties are the
141 standard deviations. The parameter α is determined through Eq. 1, i.e. dividing the slope of the
142 density vs. temperature by the density of the sample at the nominal temperature. Similarly, β_i
143 are calculated through Eq. 2, i.e. dividing the slope of the density vs. concentration by the
144 density of the sample at the nominal concentration.
145
146 ***Table 1: Thermophysical properties of the polystyrene-toluene-n-hexane mixture***

Parameter	Value
ρ	$(750.0 \pm 0.4) \times 10^{-3}$ g/cm^3
ν	$(5.24 \pm 0.01) \times 10^{-3}$ cm^2/s

α	$(9.1 \pm 0.7) \times 10^{-4}$/K
β_1	$(3.1 \pm 0.1) \times 10^{-1}$
β_2	$(2.6 \pm 0.1) \times 10^{-1}$

147

148 *2.2 Thermodiffusion experiment*

149 The experimental set-up is quite similar to the one used in previous studies and a more detailed
150 description can be found elsewhere [6, 7]. Before filling our thermodiffusion cell, its interior is
151 evacuated by using a vacuum pump for more than four hours in order to evaporate all the
152 residual fluids. Subsequently, the mixture is injected into the cell. The sample is sandwiched
153 between two square sapphire windows of 8 mm thick, mechanically separated to provide a
154 vertical thickness of the fluid layer of $L = (5.0 \pm 0.1)\ mm$. Two thermoelectric (TEC) Peltier
155 devices are used to apply the temperature gradient to the fluid mixture. Both TECs are
156 independently connected to two proportional-integral-derivative (PID) temperature controllers
157 (Wavelength Electronics, MODEL LFI - 3751), being able to set the temperatures of the two
158 sides of the fluid slab with an absolute accuracy of 0.01 K and a relative RMS stability of 1 mK
159 over 24 hours. The temperature gradient is applied in the z direction, and the sample is always
160 heated from above in order to avoid convection, since both Soret coefficients are expected to
161 be positive [44-46]. When applying a temperature gradient, the two TECs actually act as heat
162 pumps in the same direction, thus a heat exchanger flushed with water coming from a thermostat
163 (HUBER, ministate 125) removes the excess heat from the external side of the Peltier elements.
164 The thermodiffusion experiments are performed by imposing temperature differences of $\Delta T =$
165 $10, 15$ and $20\ K$ over the vertical extension of the sample cell. After imposing the temperature
166 gradient, and before starting the image acquisition through the shadowgraph setup, it is
167 necessary that the sample reaches the stationary state where the Soret effect is completely
168 balanced by Fickean diffusion. In our experimental conditions, the diffusion time $\tau = L^2/D$ is

of the order of $8.3 \times 10^4\ s$, i.e. about 23 hours. This value is obtained from the diffusion coefficient of the polymer in a typical solvent, like toluene $D \approx 3 \times 10^{-6}\ cm^2/s$ [45].

Density fluctuations $\delta\rho$ generated by both temperature fluctuations δT and concentration fluctuations $\delta\omega_i$ give rise to refractive index fluctuations $\delta n = \delta T(\partial n/\partial T) + \sum_i \delta\omega_i(\partial n/\partial\omega_i)$, which can be detected by optical techniques, as described in the literature [11, 13, 47]. In general, velocity fluctuations are not supposed to induce fluctuations of the density or of the refractive index.

In our optical setup, a super-luminous diode (Superlum, SLD-MS-261-MP2-SM) with a wavelength of $\lambda = (675 \pm 13)$ nm acts as the light source, illuminating the sample parallel to the temperature gradient. The light is provided out of a monomode optical fibre and the beam is collimated by an achromatic doublet lens with focal length $f = 150\ mm$ and placed at its focal distance from the fibre output. After the collimating lens, a linear polariser is positioned before the sample and a second linear polariser (analyser) after it, providing a control of the light intensity independent of the integration time of the detector. Finally, the light beam impinges onto a scientific-CMOS camera (Hamamatsu Digital Camera C13440, ORCA - Flash 4.0) whose detector size is s = 1.33 cm, placed in the near field, i.e. at a distance $z = (200 \pm 5)\ mm$ from the sample midplane. The s-CMOS camera allows a 'fast' image acquisition frequency up to 100Hz at full frame (2048 × 2048 pixels), thus enabling a fruitful characterization of the temperature fluctuations in the observable wave number range. The shadowgraph signal is the result of the interference of the transmitted beam with the ones scattered by the sample refractive index fluctuations. In our experiment series of $N = 2500$ images of 2048 × 2048 pixels, corresponding to $q_{min} = 2\pi/s = 4.72/cm$, are recorded for three different frequencies of $f = 100, 10, 1\ Hz$, corresponding to minimum correlation times of $dt_{min} = 0.01, 0.1, 1\ s$. The recorded images are eventually analysed by the Differential Dynamic Algorithm (DDA) briefly described in the following section [48].

194

195 *2.3 Dynamic shadowgraphy*

196 The DDA analysis consists of the following steps: images are recorded at different times as bi-
197 dimensional intensity maps $I(\vec{x},t)$ and are 2D-Fourier transformed and normalized to get
198 $i(\vec{q},t) = I(\vec{q},t)/I(0,t)$. Then, differences between pairs of normalised Fast Fourier
199 Transforms (FFTs) are calculated and their square moduli are determined $|\Delta i(\vec{q},t,dt)|^2 =$
200 $|i(\vec{q},t) - i(\vec{q},t+dt)|^2$. These quantities are computed for all possible delay times dt,
201 multiples of the dt_{min} set by the acquisition frequency of the detector. Finally, the results are
202 averaged first over time $\langle|\Delta i(\vec{q},dt)|^2\rangle = \langle|\Delta i(\vec{q},t,dt)|^2\rangle_t$ and second over the modulus of the
203 wave vector $\vec{q}$, $\langle|\Delta i(q,dt)|^2\rangle = \langle|\Delta i(\vec{q},dt)|^2\rangle_{|\vec{q}|}$. The resultant function is the so-called
204 Structure Function (SF) $\langle|\Delta i(q,dt)|^2\rangle$. All these calculations are performed by a custom
205 software running on a graphic card and taking advantage of the massive parallelization of the
206 Graphic Processing Unit (GPU), thus requiring about one hour of computational time for each
207 experiment, i.e. the three series of 2500 images of 2048 × 2048 pixels [49].

208

209 *2.4 Concatenation of the experimental structure function*

210 As mentioned above, in the experiments reported in this study, sets of images of 2048 × 2048
211 pixels have been recorded at three different acquisition frequencies at the steady state of the
212 thermodiffusion process. Then, the experimental SF is determined by analysing each stack of
213 images acquired at a specific frequency. Examples of $\langle|\Delta i(q,dt)|^2\rangle$ are shown in Fig. 1, as a
214 function of the wave number (Fig. 1a, 1c, 1e) and as a function of the correlation time dt for
215 different wave numbers (Fig. 1b, 1d, 1f). The SFs obtained at three different frequencies are
216 then merged in order to form a single concatenated SF, or c-SF (Fig. 1g), that covers a large
217 range of correlation times of about four orders of magnitude, as shown in Fig. 1h.

As stated above, the c-SF is the result of merging the SFs determined at three different frequencies (from left to right in Fig. 1h): the first points correspond to the data acquired at 100 Hz (from Fig. 1b, dark purple squares at short *dt*), the second ones to 10 Hz (from Fig. 1d, light cyan circles at intermediate *dt*) and the third ones to 1 Hz (from Fig. 1f, dark orange triangles at large *dt*). The concatenation procedure is made by simply selecting the relevant part of the SFs as shown in Fig. 1. About the 10% of the delay times of each data set are used for the concatenation, disregarding those that are already included in the slower frequency slot. This means that from the fastest acquisition set only delay times in the range 0.01-2.5 s are taken, from the intermediate one the selected range is 2.5-25 s and from the slowest one 25-250 s. The concatenation procedure has been already applied in our precedent work [43], but here it is described in more detail. We point out that this scheme becomes useful whenever it is necessary to investigate NEFs with quite different decay times and that it is similar to the multi-tau approach utilised in dynamic light scattering [50].

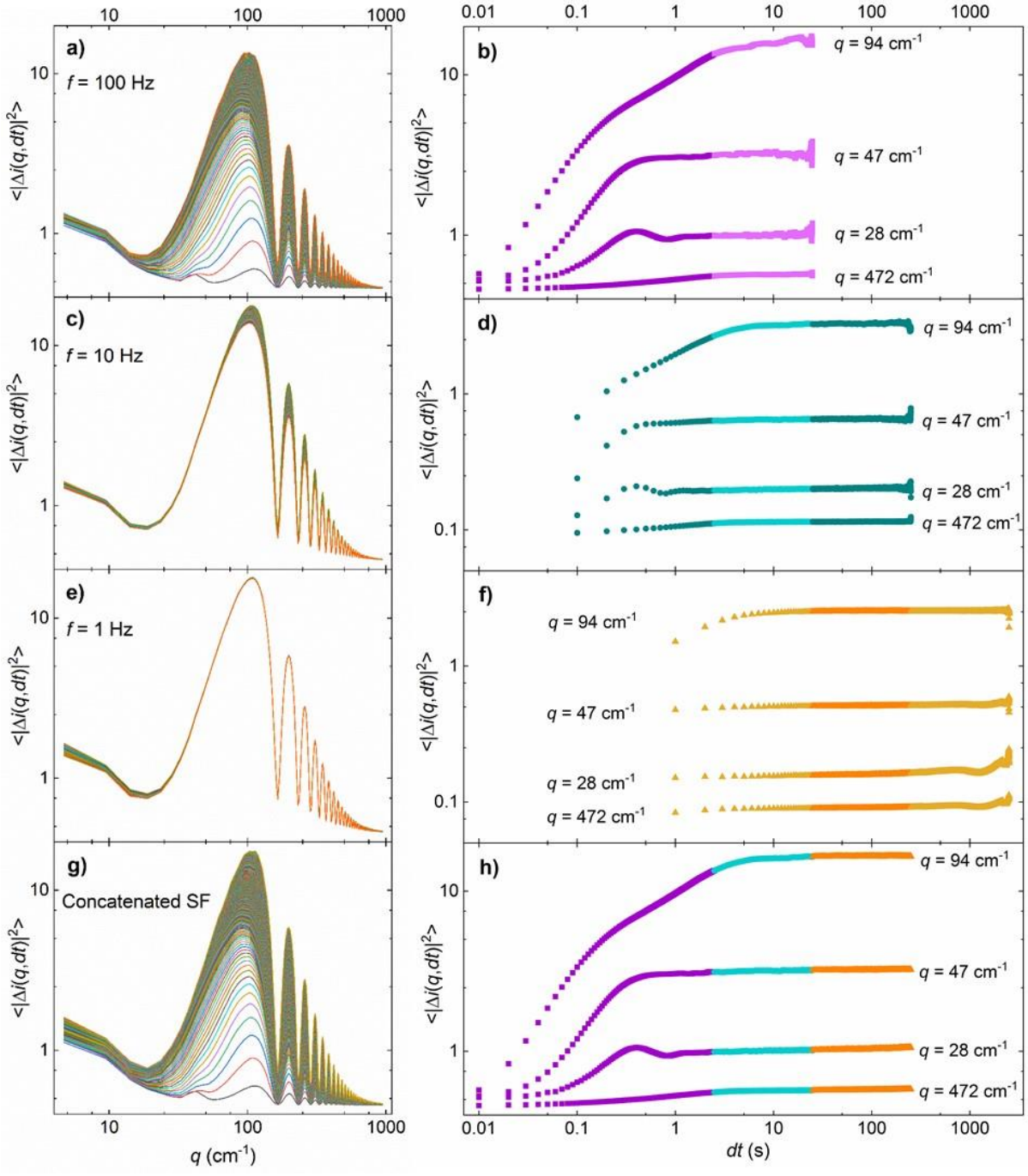

Figure 1: Structure function of the thermodiffusion experiment carried out at temperature difference of 20 K for a series of images of 2048 × 2048 pixels at 100, 10 and 1 Hz, as a function of the wave number (a, c, e, respectively) and as a function of correlation time (b, d, f, respectively). Concatenated structure function as a function of the wave number (g) and as a function of time (h). Purple squares, cyan circles and orange triangles correspond to the data acquired at 100, 10 and 1 Hz, respectively.

2.5 Analysis of experimental signals

After the DDA and the concatenation process one gets the c-SF; it represents the raw experimental signals, obtained only from the acquired image series. For the analysis of these concatenated $\langle|\Delta i(q,dt)|^2\rangle$, the physical optics theory of shadowgraph proposes the following expression [12, 48]:

$$\langle|\Delta i(q,dt)|^2\rangle = 2\{T(q)S(q)[1 - I_{SF}(q,dt)] + B(q)\}, \quad (3)$$

where $T(q)$ is the shadowgraph optical transfer function [11], $S(q)$ is the static power spectrum, $B(q)$ is the background and $I_{SF}(q,dt)$ is the intermediate scattering function, that usually is described as a sum of exponential decays: $I_{SF}(q,dt) = \sum_i a_i exp(-dt/\tau_i(q))$, where a_i are the amplitudes of the different modes (with $\sum_i a_i = 1$) and $\tau_i(q)$ the wave-number dependent relaxation times.

A simple observation of Fig. 1h, without any calculation, shows that, depending on the wave number range, up to three different decay times can be distinguished in the c-SF. In some cases, these decay times differ by more than one order of magnitude. In addition, and also depending on the wave number range, one can observe in Fig. 1h damped oscillations in $\langle|\Delta i(q,dt)|^2\rangle$. This oscillating (propagating) phenomenon means that at least two of the relaxation times $\tau_i(q)$ present in the $I_{SF}(q,dt)$ of Eq. 3 (and their associated amplitudes) form a pair of complex conjugate numbers. We conclude that a complex scenario of NEFs with different decay times is present in the case of a ternary mixture with large Le and Dr numbers, and a key question is the selection of the number of modes in the $I_{SF}(q,dt)$ of Eq. 3 and whether they are purely diffusive (monotonically decaying) or propagating (oscillating). A rational choice needs to be guided by the available theoretical models for NEFs in ternary mixtures, which we review next.

3. Theoretical framework

3.1 Thermodiffusion in ternary mixtures

In a ternary mixture, the mass concentrations of the three components are related by: $\omega_1 + \omega_2 + \omega_3 = 1$, which means that only two concentrations, e.g. ω_1 and ω_2, are independent. The corresponding diffusion fluxes J_1 and J_2 in the centre-of-mass frame of reference have thermodiffusion and Fickean components, as expressed by [51]:

$$\begin{pmatrix} J_1 \\ J_2 \end{pmatrix} = -\rho \left[\begin{pmatrix} D_{11} & D_{12} \\ D_{21} & D_{22} \end{pmatrix} \begin{pmatrix} \nabla\omega_1 \\ \nabla\omega_2 \end{pmatrix} + \begin{pmatrix} \omega_1(1-\omega_1) & -\omega_1\omega_2 \\ -\omega_1\omega_2 & \omega_2(1-\omega_2) \end{pmatrix} \begin{pmatrix} \mathrm{D}_{T1} \\ \mathrm{D}_{T2} \end{pmatrix} \nabla T \right], \quad (4)$$

where ρ is the density of the mixture, D_{ij} are the components of the centre-of-mass diffusion matrix, $\nabla\omega_i$ are the concentration gradients, D_{T_i} are the invariant thermodiffusion coefficients and ∇T is the applied temperature gradient.

At the stationary state, the diffusion fluxes become zero and, following Ortiz de Zárate [51], the Soret coefficients S_{T_i} can be expressed by:

$$\begin{pmatrix} \omega_1(1-\omega_1) & -\omega_1\omega_2 \\ -\omega_1\omega_2 & \omega_2(1-\omega_2) \end{pmatrix} \begin{pmatrix} \mathrm{S}_{T1} \\ \mathrm{S}_{T2} \end{pmatrix} \nabla T = -\begin{pmatrix} \nabla\omega_1 \\ \nabla\omega_2 \end{pmatrix}, \quad (5)$$

The introduction of the matrix concentration pre-factors in Eqs. 4 and 5 forces the thermodiffusion coefficients D_{T_i} and the Soret coefficients S_{T_i} to display the same frame-invariance properties of the single D_T or S_T of a binary mixture, that is, they are numerically the same irrespective of whether mass fractions or mole fractions are used to express the composition [51]. Here, for simplicity, we display the equations only in the mass fraction framework.

Fluctuating Hydrodynamics (FHD) has been recently extended to ternary mixtures first considering equilibrium fluctuations [52] and then non-equilibrium fluctuations [39, 40]. The first NE theory [39] neglected the effects of gravity and confinement. In that case, there is no mixing between the decay rates of the four hydrodynamic modes (fluctuations of velocity, temperature and two concentrations) which continue to decay with their well-known equilibrium values given by kinematic viscosity, thermal diffusivity and the two eigenvalues

$\widehat{D}_i$ of the diffusion matrix **D**. These $\widehat{D}_i$, are always real and positive, and can be related to the four components D_{ij} of Eq. 4 by [39, 40]:

$$\widehat{D}_{1,2} = \frac{1}{2}\left[D_{11} + D_{22} \mp \sqrt{(D_{11} - D_{22})^2 - 4D_{12}D_{21}}\right]. \quad (6)$$

In accordance with the aforementioned common notation (i.e. 1 for PS, 2 for toluene and 3 for n-hexane), $\widehat{D}_1 < \widehat{D}_2$ since $\widehat{D}_1$ represents the slowest diffusion mode essentially related to the diffusion of the polystyrene in the binary solvent.

Since refractive index does not depend on fluid velocity, only three of the four hydrodynamic modes are directly observable by optical techniques. Hence, within the approximations of Ref. [39] (no gravity and no confinement) we conclude that for a thermodiffusion experiment in a ternary mixture, a suitable expression for the $I_{SF}(q, dt)$ can be provided by the sum of three exponential decays given by two concentration modes, plus one mode for temperature fluctuations:

$$I_{SF}(q, dt) = a_1 \exp[-dt/\tau_1(q)] + a_2 \exp[-dt/\tau_2(q)] + (1 - a_1 - a_2)\exp[-dt/\tau_3(q)], \quad (7)$$

where a_i are the normalised amplitudes of the different modes and $\tau_i(q)$ the corresponding relaxation times.

3.2 Concentration NEFs in ternary mixtures including gravity effects

For NEFs, first the theory was developed in the absence of gravity force [39]; while gravity effects were incorporated by Martínez Pancorbo et al. [40]. Both of these papers adopted the so-called large Lewis number approximation that uncouples temperature fluctuations from concentration fluctuations. Next, we briefly summarize the main results of Ref. [40] and recall the expressions useful for the experimental data analysis.

The presence of gravity causes a mix between the two concentrations NEFs. The corresponding decay times can be described as $\tau_i(q) = 1/[\gamma_i(q)q^2]$, where the diffusivities $\gamma_i(q)$ in dimensionless form, are given by the following equation [40]:

$$\gamma_i(\tilde{q}) = \frac{1}{2}\left(\widehat{D}_1 + \widehat{D}_2 - \frac{Ra_i\widehat{D}_i}{\tilde{q}^4}\right) \times \left[1 \mp \sqrt{1 - \frac{\frac{4\widehat{D}_1\widehat{D}_2}{(\widehat{D}_1+\widehat{D}_2)^2}\left[1-\frac{Ra_{S,ter}}{\tilde{q}^4}\right]}{\left[1-\frac{Ra_i\widehat{D}_i}{\tilde{q}^4(\widehat{D}_1+\widehat{D}_2)}\right]^2}}\right], \quad (8)$$

where $\tilde{q} = qL$ is the dimensionless wave number, and Ra_i are the two solutal Rayleigh numbers defined for ternary mixtures by:

$$Ra_i = \frac{gL^4}{\nu\widehat{D}_i}\beta'_i\nabla\omega'_i, \quad (9)$$

$$Ra_i\widehat{D}_i = Ra_1\widehat{D}_1 + Ra_2\widehat{D}_2, \quad (10)$$

$$Ra_{S,ter} = Ra_1 + Ra_2, \quad (11)$$

In Eq. 9, the primes indicate the concentrations (mass fractions) in which the diffusion matrix is diagonal, for a generic diffusion matrix [53]:

$$\begin{pmatrix}\omega'_1\\ \omega'_2\end{pmatrix} = \begin{pmatrix}1 & \frac{D_{22}-\widehat{D}_2}{D_{21}}\\ \frac{D_{11}-\widehat{D}_1}{D_{12}} & 1\end{pmatrix}\begin{pmatrix}\omega_1\\ \omega_2\end{pmatrix}. \quad (12)$$

The use of "diagonal" concentrations simplifies the theory but, as we shall see, somewhat complicates the interpretation of experimental results. In general, they differ from the measurable mass fractions.

In summary, in this model [40] the two concentration modes couple, while temperature fluctuations remain uncoupled, keeping their equilibrium decay rate unaltered. Since for typical values of Ra_i the two decay times of Eq. 8 are real numbers, this theory [40] suggests to still use Eq. 7 for the $I_{SF}(q, dt)$. We note that the notation of Eqs. 9-11 implies that, for a ternary mixture, two Lewis numbers (Le_1 and Le_2) can be defined as $Le_i = a_T/\widehat{D}_i$.

3.3 Coupling of concentration and temperature NEFs in binary mixtures

In the simplest case of binary mixtures, most of the available literature on concentration and temperature NEFs makes use of the simplification that the two modes are always decoupled. This is essentially true whenever the large Lewis number approximation is valid, that is the case of ordinary liquid mixtures whose mass diffusion coefficient is much smaller than the thermal diffusivity. However, the decoupling assumption fails to be valid for very large fluctuations, i.e. for small wave numbers, as recently demonstrated both experimentally and theoretically [43]. In particular, only the full coupling of velocity, temperature and concentration NEFs in the bulk fluid can explain the appearance of propagating modes giving rise to a $I_{SF}(q,dt)$ that includes oscillations at very small wave numbers. This mechanism also induces a slowing-down of the non-propagating concentration NEFs similar to that caused by the confinement effect [41, 42].

This theory of full coupling between NE velocity, temperature and concentrations fluctuations has been published only for binary mixtures. We briefly recall here the main steps of the theoretical framework, while for details we address the reader to the literature [43].

In order to take into account a more complete description of the behaviour of NEFs within a thermodiffusion experiment, one should write the evolution equations of the fluctuations of velocity v_z, temperature and concentration of the single independent component:

$$\frac{\partial}{\partial t}\begin{bmatrix}\delta v_z(q,t)\\ \delta T(q,t)\\ \delta\omega(q,t)\end{bmatrix} = -\mathbf{G}(q)\begin{bmatrix}\delta v_z(q,t)\\ \delta T(q,t)\\ \delta\omega(q,t)\end{bmatrix}, \tag{13}$$

where the inverse linear response matrix in its dimensionless form can be written as:

$$\mathbf{G}(\tilde{q}) = \begin{bmatrix} PrLe\tilde{q}^2 & -1 & 1\\ -Ra_s PrLe/\psi & Le\tilde{q}^2 & 0\\ Ra_s PrLe & \psi\tilde{q}^2 & \tilde{q}^2\end{bmatrix}, \tag{14}$$

In the previous equation the well-known dimensionless numbers appear, namely the Lewis number $Le = a_T/D$, where a_T is the thermal diffusivity; the Prandtl number $Pr = \nu/a_T$; the

separation ratio $\psi = c_0(1-c_0)S_T\beta/\alpha$; and the solutal Rayleigh number $Ra_S = [\beta g \nabla\omega/(\nu D)]L^4$.

The solution of Eqs. 13 and 14 requires the computation of the eigenvalues and eigenvectors of the matrix $\mathbf{G}(\tilde{q})$:

$$\det[\mathbf{G}(\tilde{q}) - \lambda\mathbf{1}] = \left[\Gamma_{v_z}(\tilde{q}) - \lambda\right][\Gamma_T(\tilde{q}) - \lambda][\Gamma_\omega(\tilde{q}) - \lambda], \quad (15)$$

with NE fluctuations dimensionless decay times given by $\tau_i(\tilde{q}) = 1/[\Gamma_i(\tilde{q})]$. Although Eq. 15 can be solved analytically, the resulting expressions of the roots as a function of q are so complicated that, in practice, it is more useful to have a numerical solution for fixed values of the parameters Pr, Le , Ra_S and ψ, in the whole range of q.

Depending on the parameter values and on the wave number q, Eq. 15 may have a pair of complex conjugate solutions, which typically happens at small q values. The resulting $I_{SF}(q,dt)$ function in those cases shows a sinusoidal term:

$$I_{SF}(q,dt) = a_1 \exp[-dt/\tau_1(q)] + \left\{\frac{1-a_1}{\cos[\phi(q)]}\right\}\cos[\Omega(q)dt + \phi(q)]\exp[-dt/\tau_2(q)]$$

, (16)

where $\Omega(q)$ is the oscillation frequency and $\phi(q)$ a phase term.

3.4 Coupling of concentration and temperature NEFs in ternary mixtures

The next step in the development of FHD is to include all the couplings among the fluctuating modes for a ternary mixture. Of course, in that case one needs to consider the evolution of fluctuations in velocity δv_z, temperature and concentration of the two independent components:

$$\frac{\partial}{\partial t}\begin{bmatrix}\delta v_z(q,t)\\ \delta T(q,t)\\ \delta\omega_1(q,t)\\ \delta\omega_2(q,t)\end{bmatrix} = -\mathbf{G_t}(q)\begin{bmatrix}\delta v_z(q,t)\\ \delta T(q,t)\\ \delta\omega_1(q,t)\\ \delta\omega_2(q,t)\end{bmatrix}, \quad (17)$$

where the inverse linear response matrix for "diagonal" concentrations can be written in dimensionless form as:

$$\mathbf{G_t}(\tilde{q}) = \begin{bmatrix} PrLe_t\tilde{q}^2 & -1 & 1 & 1 \\ -PrLe_t{}^2Ra & Le_t\tilde{q}^2 & 0 & 0 \\ PrLe_t{}^2Ra\psi_1' & \psi_1'\tilde{q}^2 & \tilde{q}^2 & 0 \\ PrLe_t{}^2Ra\psi_2' & Dr\psi_2'\tilde{q}^2 & 0 & Dr\tilde{q}^2 \end{bmatrix}. \quad (18)$$

To make dimensionless Eqs. 17 and 18, L is used as unit of length and $L^2/\widehat{D}_1$ as unit of time; consequently, $\tilde{q} = qL$ for wave numbers, and $L/\widehat{D}_1$ is the unit of velocity. Hence, everything is made dimensionless with respect to the slower diffusive mode. Other dimensionless parameters in Eq. 18 are: one (unique) ternary Lewis number $Le_t = a_T/\widehat{D}_1$, the Diffusion eigenvalue Ratio $Dr = \widehat{D}_2/\widehat{D}_1$, the thermal Rayleigh number $Ra = -\alpha g L^4 \nabla T/(\nu a_T)$ and the "diagonal" separation ratios $\psi_i' = D_{T,i}^{\omega\prime}\beta_i'/(\widehat{D}_i\alpha)$, with $D_{T,i}^{\omega\prime}$ being the (diagonal) thermodiffusion coefficients as defined in Ref. [18]. We point out that this approach is different from the one used in our previous publication [40] and reported in section 3.2, where two Lewis numbers were introduced.

As in the case of binary mixtures, the solution of Eq. 17 requires to numerically evaluate the dimensionless decay rates $\Gamma_i(\tilde{q})$ as the four eigenvalues of the matrix $\mathbf{G_t}(\tilde{q})$, namely:

$$\det[\mathbf{G_t}(\tilde{q}) - \lambda\mathbf{1}] = \left[\Gamma_{\nu_z}(\tilde{q}) - \lambda\right][\Gamma_T(\tilde{q}) - \lambda]\left[\Gamma_{\omega_1}(\tilde{q}) - \lambda\right]\left[\Gamma_{\omega_2}(\tilde{q}) - \lambda\right]. \quad (19)$$

A more detailed explanation of the full-coupling theory for ternary mixtures is outside the scope of the present publication and will be the subject of a future paper. We simply mention that, depending on q, complex solutions of Eq. 19 may exist. As was the case with binaries, for parameter values typical of ternary liquid mixtures, these propagating modes do appear as a mixing between the temperature and the viscous (velocity) modes. The consequence is an oscillatory $I_{SF}(q, dt)$ such as the one expressed in Eq. 16, but with an additional exponential term to represent the extra concentration mode.

4. Results

400 *4.1 Intermediate scattering function analysis*

401 As mentioned in section 2.5, for most wave numbers the $I_{SF}(q, dt)$ of Eq. 3 is usually defined
402 as a sum of exponential decays. However, a preliminary analysis of the experimental SF is
403 required to check the suitability of this model. As it can be seen in the c-SF shown in Fig. 1h
404 for $q = 94/cm$, three exponential decays can be detected, corresponding (from left to right) to
405 the relaxation of the temperature and concentration (faster and slower mass modes) NEFs.
406 Then, the $I_{SF}(q, dt)$ can be modelled for most wave numbers by a sum of three exponential
407 decays, as defined in section 3.1 by Eq. 7 for a system including one thermal mode plus two
408 solutal, well separated, modes. In the studied system, the corresponding three exponential
409 decays represent the following three modes: long decay times for the two concentration modes,
410 slower for mass diffusion of the denser component (PS in the binary solvent), and faster for
411 mass diffusion of the two components of the solvent mixture (toluene and n-hexane); and the
412 shortest decay time corresponds to the thermal diffusivity of the overall mixture.

413 Nevertheless, for small wave numbers such as $q = 28/cm$, oscillations are detected in the c-
414 SF (see Fig. 1h), indicating the presence of propagating modes [43]. Fig. 2 shows the
415 oscillations in the experimental c-SF for several wave numbers in the range $19/cm < q <$
416 $47/cm$. These need to be taken into account by using a proper $I_{SF}(q, dt)$ function, such as the
417 one described in section 3.3 by Eq. 16. The latter equation is defined for a binary mixture, and
418 includes one solutal mode, i.e. the exponential decay, and a coupled thermo-viscous mode, i.e.
419 the damped oscillation. For analysing ternary mixtures, one should supplement Eq. 16 with an
420 additional exponential term, representing the second solutal mode. However, after carrying out
421 a careful comparison of the corresponding fitting output, we have found that the addition of this
422 term gives more scattered results due to the increase in the number of fitting parameters. For
423 that reason, Eq. 16 has been used to fit the raw data in the wave number range where oscillations

are detected in the c-SF. The slower concentration mode is, thus, unobservable in this wave number range.

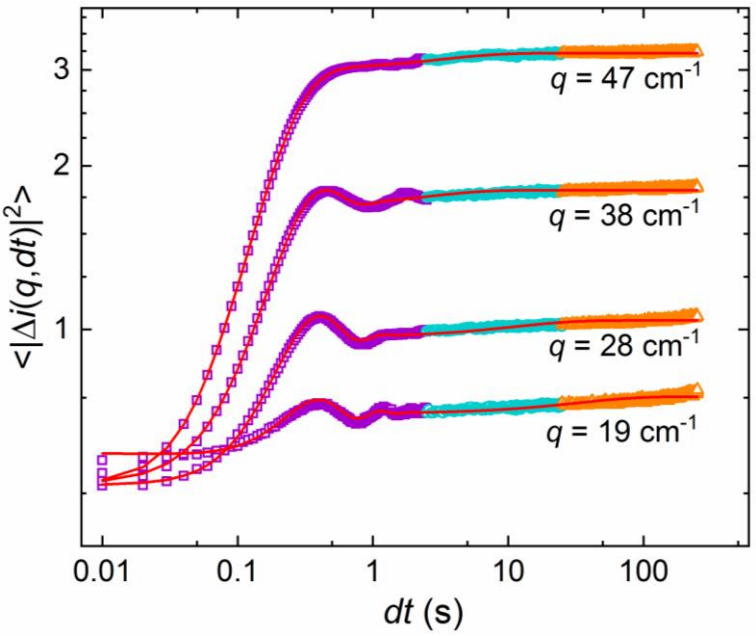

Figure 2: Concatenated structure function of the thermodiffusion experiment carried out at temperature difference of 20 K for a series of images of 2048 × 2048 as a function of time for different small wave numbers. Purple squares, cyan circles and orange triangles correspond to the data acquired at 100, 10 and 1 Hz, respectively, and the red curves to the fitting functions through Eqs. 3 and 16.

Generally, the quality of these fittings is good, as demonstrated in Fig. 2, with an average R^2 of about 0.99, which translates into a 3% mean relative uncertainty for the decay times determined by these fittings. However, both R^2 and the relative uncertainty of the decay times depend on the wave number. The best accuracy is obtained for intermediate wave numbers where the signal-to-noise ratio of the c-SF is the largest (see Fig. 1g). Decay times with a relative uncertainty larger than 10% have been disregarded for the further analysis.

4.2 Decay times of the NEFs

Figure 3 shows the decay times of the different fluctuating modes as resulting from the modelling of the experimental c-SF by using Eqs. 3 and Eq. 7 or Eq. 16 depending on the analysed q. Three decay times are easily distinguished (from top to bottom): the slowest mode (black symbols) describes the concentration mode of the polymer into the binary solvent; the intermediate one (blue symbols) the concentration mode of the binary solvent mixture; and the fastest one (red symbols) the temperature mode. These decay times cover a span of about three orders of magnitude, which is quite impressive for an imaging technique. This justifies the necessity of performing measurements at different acquisition frequencies and of carrying out the concatenation procedure adopted here. Besides decay times, when the Eq. 16 is used, the fitting procedure also gives the oscillation frequency $\Omega(q)$ of the propagating modes appearing in Fig. 2 for wave numbers $q < 47/cm$.

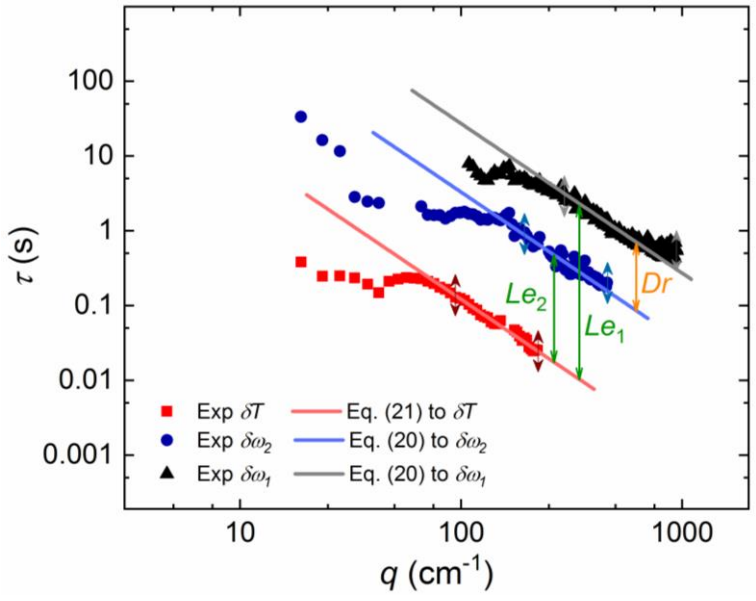

Figure 3: Decay times of NEFs on the ternary mixture of PS-toluene-n-hexane in a thermodiffusion experiment performed at temperature difference of 20 K, as a function of the wave number q. Lines represent fitting functions through Eqs. 20-21 over the diffusive wave number range, as indicated in the text.

The experimental decay times shown in Fig. 3 are to be discussed first in the diffusive regime only (for large enough wave numbers), where the three decay times are well-separated. As elucidated at the end of section 3.1, in this region of large wave numbers the effect of gravity is negligible for both concentration modes, and the decay times of the two concentration modes are given by the eigenvalues of the diffusion matrix:

$$\tau_i(q) = 1/\left(\widehat{D}_i q^2\right). \tag{20}$$

By fitting the experimental decay times in the diffusive regime ($q > 290/cm$ for the concentration NEFs, c-NEFs, of component 1 and $q > 190/cm$ for the c-NEFs of component 2) to Eq. 20, the eigenvalues of the diffusion matrix can be determined. The diffusion coefficient $\widehat{D}_1$ obtained from the slowest concentration mode represents the mass diffusion eigenvalue of the polymer in the binary solvent mixture. $\widehat{D}_2$ calculated from the intermediate decay times (i.e. faster concentration mode) represents the mass diffusion eigenvalue of toluene in n-hexane (i.e. interdiffusion of the solvents in the solvent mixture). The resulting two eigenvalues $\widehat{D}_1$ and $\widehat{D}_2$ are reported in Table 2. These values in Table 2 are calculated by averaging the fitting results of the experiments performed at three temperature differences, 20, 15 and 10 K, and the uncertainties are the corresponding standard deviations. These values are comparable with those obtained in our previous study [14] for a similar polymeric mixture prepared with the same components of this study but a slightly different polymer molecular weight, and with those reported in [43, 45] for the diluted binary mixture of PS-toluene and in [44, 46] for the binary solvent mixture of toluene-n-hexane. Furthermore, the value of the Dr number can be determined as the ratio between the two eigenvalues, resulting in $Dr = 8.4$ (see Table 2). This value totally justifies the selection of the polymeric mixture as a suitable sample for experimentally studying well-separated concentration modes.

In a similar way, in order to get information about the thermal diffusivity a_T of the ternary mixture, one can try to fit the data points of the thermal mode with the theoretical predictions

for thermal NEFs only. In the diffusive regime, the decay time of the thermal mode can be expressed as [54]:

$$\tau_{th}(q) = 1/(a_T q^2), \quad (21)$$

and the fitting of temperature NEFs for $q > 90/cm$ in Fig. 3 provides the thermal diffusivity value reported in Table 2. This result is again comparable with the one obtained in previous studies for a similar polymeric mixture [14] as well as with that reported in [46] for the equi-molar toluene-n-hexane binary solvent mixture.

From the two diffusion eigenvalues and the thermal diffusivity, the Le_i numbers can be determined, which are also listed in Table 2.

Table 2: Diffusion coefficient eigenvalues, Le_i and Dr numbers of the polymeric ternary mixture

Parameter	Value
$\widehat{D}_1$	$(3.8 \pm 0.1) \times 10^{-6}$ cm^2/s
$\widehat{D}_2$	$(3.1 \pm 0.1) \times 10^{-5}$ cm^2/s
a_T	$(8.5 \pm 0.2) \times 10^{-4}$ cm^2/s
Le_1	227 ± 12
Le_2	27 ± 2
Dr	8.4 ± 0.6

5. Discussion

Comparison between experimental and theoretical decay times

As described in section 3.2, Martínez-Pancorbo et al. [40] presents the analysis of the fluctuations of two independent concentrations together with the effect of buoyancy, but considering neither the effect of confinement nor the presence of temperature and velocity

fluctuations. Consequently, the coupling between modes which is known to be important at small wave numbers, as demonstrated for binary mixtures [43], is not taken into account. In order to be insensitive to confinement effects the experiments reported here have been performed in a thick cell with vertical dimension of $L = 5\ mm$. In these conditions, the effect of confinement should not be visible in the investigated wave number range. In fact, confinement effects appear only at dimensionless wave numbers $\tilde{q} = qL < 5$, corresponding here to dimensional wave numbers $q < 10/cm$, at the very bottom of the investigated range of q [41, 42].

Regarding coupling effects, it is mandatory to consider them whenever oscillations are visible in the experimental c-SF at small q (see Fig. 2). The complete FHD theory, including the presence of velocity and temperature fluctuations and the various couplings among all modes, has been previously published by us [43] for the case of binary mixtures, as summarised in section 3.3. The results of [43] can be very useful for discussing the impact of the velocity-temperature coupling on the measured decay times.

In the following, we compare the experimental values of decay times at different wave numbers (obtained by fitting the c-SF through Eqs. 3 and 7 or 16), with the two published models [40, 43]. This allows to understand the impact of the different effects on the measured c-SF, and to evaluate if a more complete theoretical framework is needed or if on the contrary, the available theories can be simply applied in different wave number ranges in order to extract the transport properties of the investigated ternary mixture. As described in the previous section, at least the diffusion coefficients can be safely determined by fitting decay times at large wave numbers, where NEFs are dominated only by the diffusion phenomenon. The measurement of the Soret coefficient is more complicated as it requires the analysis of the effect of gravity [6], or other suitable analysis [55]. The simultaneous and independent characterization of the two Soret coefficients of a ternary mixture requires a complete knowledge of the diffusion matrix

including the cross-diffusivities. This has not been achieved yet by Shadowgraphy and is the ultimate goal of our current research. Although we estimate that this can be done with one-wavelength Shadowgraphy, a more precise information can be obtained with a two-wavelength version of the technique. The two-wavelength Shadowgraphy is currently being developed in our lab, also in relation to the future space experiments of the NEUF-DIX project [28].

Figure 4 shows the experimental decay times and the oscillation frequency obtained from the c-SF (data points are the same as in Fig. 3), together with theoretical predictions provided either by Eq. 8 (dashed yellow curves) or by numerically solving Eqs.14-15 (solid green curves).

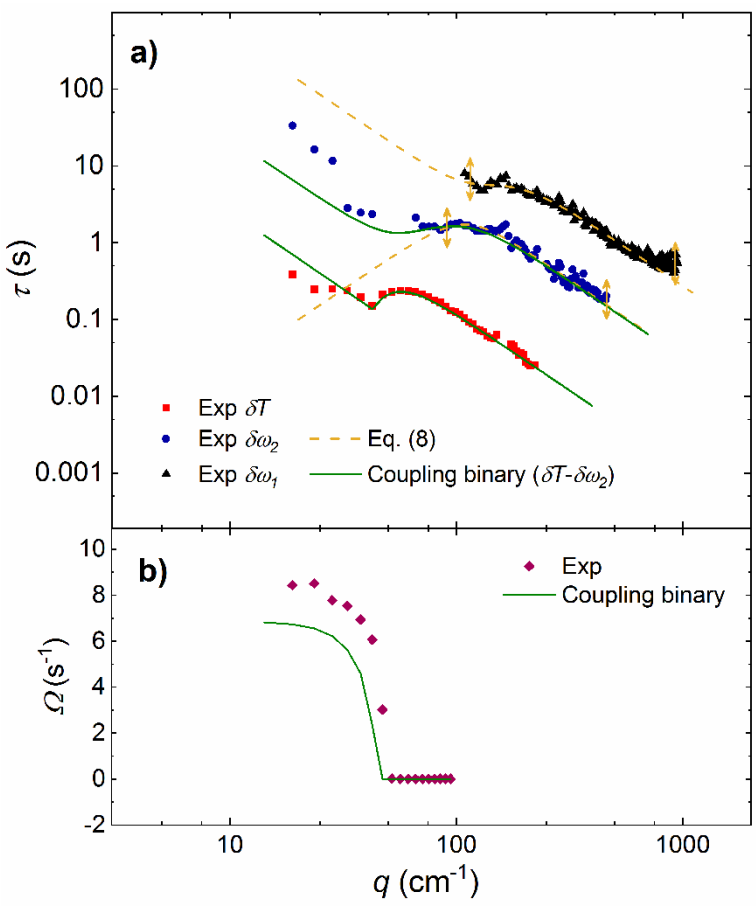

Figure 4: a) Decay times and b) oscillation frequency of NEFs on the ternary mixture of PS-toluene-n-hexane in a thermodiffusion experiment performed at temperature difference of 20 K, as a function of the wave number q. Experimental data are shown by points, while lines

represent the numerical calculations of Eqs. 8 (dashed lines) and the theory developed for binary mixtures including the effect of propagating modes (solid lines).

The experimental data are fitted to Eq. 8 by fixing the diffusion matrix eigenvalues ($\widehat{D}_1$ and $\widehat{D}_2$) to the corresponding values presented in Table 2. The parameters obtained from this fitting to Eq. 8 are: $Ra_i\widehat{D}_i = (260 \pm 40)\ cm^2/s$, and $Ra_{S,ter} = (4.6 \pm 1.0) \times 10^7$. As visible in Fig. 4a, the experimental results suggest that the available theory for the ternary mixture reported by Martínez Pancorbo et al. [40] cannot describe the behaviour of c-NEFs in the present experiment for the whole range of wave numbers. The theory provides suitable predictions for intermediate and especially for large wave numbers, but fails in the limit of small q (in particular for the fastest concentration mode) where the effect of the coupling with temperature fluctuations, and the consequent appearance of propagating modes in the experimental structure function become significant (see section 3.3) [43]. Hence, investigation of the coupling with temperature fluctuations is required for a full understanding of the present experimental results. We proceed into two steps: first we compare with the published theory [43] for the binary mixture case (one concentration mode) as reviewed in section 3.3; second we compare with the theory for ternary mixtures (two concentration modes) as briefly presented here in section 3.4. This allows appreciating the features that are genuinely related to the ternary mixture case.

As already mentioned, Fig. 4 shows, superposed on the experimental data, the theoretical predictions (green solid lines) of the theory [43] with one concentration mode. The theoretical curves have been obtained numerically (solving Eqs. 14 and 15) by keeping constant the Lewis number $Le = 27$ to the same value of Le_2 shown in Table 2, and varying the values of Pr and ψ to best fit the data. The solutal Rayleigh number $Ra_{S,2} = -\left(q_{S,2}^* L\right)^4$ is also kept constant at -5.8×10^6, after evaluating the value of the solutal rolloff wave number $q_{S,2}^*$. This value represents the wave number where the fluctuation $\delta\omega_2$ behaviour changes from diffusive to

565 gravitational [6]. The resulting values for the free fitting parameters are the following: $Pr =$
566 9.0 and $\psi = 0.9$. As it can be observed in Fig. 4a, the decay times provided by the numerical
567 solution agree very well with the experimental decay times of the temperature NEFs in the
568 whole range of wave numbers. However, for the diffusion mass mode, at the smallest wave
569 number range, the agreement is not as good as for the temperature, and a slowing-down of the
570 experimental decay times is visible in comparison to the corresponding numerical solution
571 (green solid line). The theoretical results of the oscillation frequency are likewise similar to the
572 experimental data (see Fig. 4b). This last comparison between the experimental and theoretical
573 decay times shows the importance of including temperature fluctuations in the theoretical
574 analysis.
575 Next, we finally take into account the more complete theory of NEFs, which includes the
576 coupling of thermal and viscous fluctuations to the two independent concentration modes
577 present in a ternary mixture, as briefly described in section 3.4. The comparison between
578 experimental and theoretical decay times is shown in Fig. 5. The effect of considering the two
579 concentration modes and the associated couplings is evident by comparing Fig. 4 and 5.

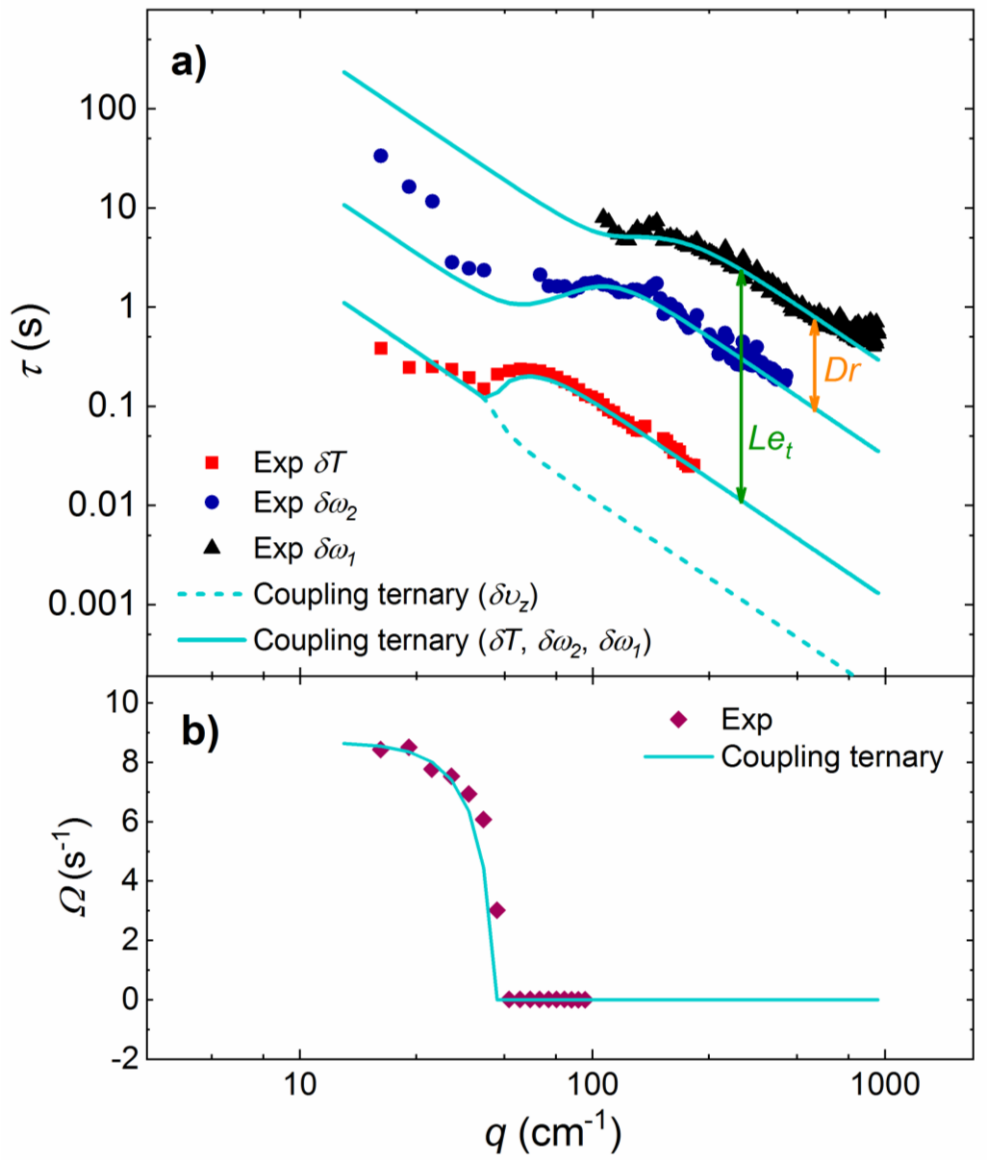

Figure 5: a) Decay times and b) oscillation frequency of NEFs on the ternary mixture of PS-toluene-n-hexane in a thermodiffusion experiment performed at temperature difference of 20 K, as a function of the wave number q. Experimental data are shown by points, while lines represent the theory developed for ternary mixtures including the effect of propagating modes.

The theoretical curves shown in Fig. 5 have been obtained numerically (solving Eqs. 18 and 19) by keeping constant $Le_t = 227$ and Dr = 8.4 (the Le_1 and Dr values shown in Table 2), and varying the values of Pr, ψ_1' and ψ_2' to best fit the data. Additionally, the term $PrLe_t{}^2Ra =$

590 $\alpha g L^4 \nabla T / \widehat{D}_1{}^2$ appearing in the matrix $G_t(\tilde{q})$ of Eq. 18 is also kept fix at 1.6×10^{11}, considering
591 for this number the α value of Table 1, the $\widehat{D}_1$ value of Table 2, and the applied temperature
592 gradient. The resulting values for the free fitting parameters are the following: $Pr = 10$, $\psi_1' =$
593 0.7 and $\psi_2' = 0.4$. The theoretical results show that for large wave numbers ($q \geq 47 cm^{-1}$), four
594 real solutions are obtained, demonstrating that all the modes are decoupled in this wave number
595 range. The velocity mode cannot be observed experimentally, as it does not give rise to
596 refractive index fluctuations. For small wave numbers ($q < 47 cm^{-1}$), two real solutions and a
597 pair of complex conjugate ones are obtained numerically, indicating that velocity and
598 temperature fluctuations are mixed at small q. This mixing induces the appearance of
599 propagating modes, observed in the experimental c-SF of Fig. 2 as oscillations at small q.
600 Applying the full theory of section 3.4, we found a reasonable agreement between the
601 experimental and the theoretical data for the three modes, especially for large and intermediate
602 wave numbers. However, we would like to point out that the numerical values of Pr, ψ_1' and
603 ψ_2' must be taken into account with caution as the fitting procedure is not robust. The focus here
604 is mainly on the qualitative understanding of the behaviour of the different modes in a ternary
605 mixture when the coupling among them is included.
606 One relevant point is the slowing-down of the two concentration modes and their consequent
607 diffusive-like behaviours at very small wave numbers (see Fig. 5a). In addition, it is worth
608 noting the good agreement obtained for the frequency of the propagating mode, as can be seen
609 in Fig. 5b. It clearly improves the results of the binary model shown in Fig. 4b.
610 Of course, the effect of confinement should be also included in the theory if one wants to
611 describe layers of ternary mixtures of any vertical thickness. Unfortunately, this additional
612 development requires more effort and no analytical solution can be obtained.
613

614 **6. Conclusions**

615 The concentration and temperature NEFs in a thermodiffusion experiment of a ternary mixture
616 composed of polystyrene, toluene and n-hexane are characterized by dynamic shadowgraphy.
617 The decay times of the NEFs are determined and three modes are clearly distinguished. The
618 fastest decay times are associated to the temperature NEFs, the intermediate ones to the
619 concentration NEFs of the molecular solvent and the slowest ones to the concentration NEFs
620 of the polymer. To encompass the very different decay times (i.e. large range of correlation
621 times), images are acquired at various frequencies, and the corresponding SFs are merged into
622 the so-called c-SF by following the described concatenation procedure.
623 In order to exploit the obtained decay times, first, they are fitted with a simple diffusive model
624 at large wave numbers to obtain the diffusion eigenvalues $\widehat{D}_1$ and $\widehat{D}_2$ and the thermal diffusivity
625 a_T. Secondly, the theory developed for the two concentration modes of a ternary mixture in the
626 presence of gravity is compared with the experimental results for the first time. The
627 experimental decay times of the concentration modes at intermediate and large wave numbers
628 appear to be in good agreement with this theoretical model. However, for smaller wave
629 numbers, a slowing-down of the experimental decay times of NEFs is detected with respect to
630 the predictions of that theory. Due to the large thickness of the thermodiffusion cell,
631 confinement effects cannot be considered as the origin of such discrepancy. In addition,
632 evidence of propagating modes on the structure function suggests that the aforementioned
633 slowing-down could be originated by the coupling of the temperature and viscous modes to the
634 concentration ones. Comparison with the decay times from the theory developed to describe
635 such coupling in a binary mixture shows a better agreement for the thermal and the faster
636 concentration modes at intermediate wave numbers. This positive outcome lead us to further
637 develop the theory of NEFs in the case of ternary mixtures, by including the coupling of
638 velocity, temperature and the two concentration modes under strong gravitational stabilization

and for large size fluctuations (small wave numbers). A better qualitative agreement is found between the new theoretical development and the experimental data points.

Acknowledgements

The authors of the University of Pau kindly thank the financial support from the Centre National d'Etudes Spatiales (CNES) and from the funding partners of the Industrial Chair CO2ES: E2S-UPPA, TOTAL, CNES and BRGM. L. García-Fernández gratefully acknowledges the CNES for the post-doctoral research grant. The research at the Complutense University was supported by grant ESP2017-83544-C3-2-P of the Spanish *Agencia Estatal de Investigación*.

Authors contribution statement

The experimental measurements and data analysis were performed by L. García-Fernández, H. Bataller and F. Croccolo. P. Fruton contributed to the concatenation procedure of the Structure Function. J.M. Ortiz de Zárate and L. García-Fernández focused on the new theoretical development presented in section 3.4. All the authors contributed to the discussion of the results and in writing the manuscript.

References

[1] F. Montel, J. Bickert, A. Lagisquet and G. Galliéro, J. Petrol. Sci. Eng., **58**, 391 (2007).

[2] H. Guo, Q. Zhou, Z. Wang and Y. Huang, Int. J. Heat Mass Tran., **117**, 966 (2018).

[3] J. M. Ortiz de Zarate and J. V. Sengers, Hydrodynamic Fluctuations in Fluids and Fluid Mixtures, Elsevier, Amsterdam, (2006).

[4] F. Croccolo, J. M. Ortiz de Zarate and J. V. Sengers, Eur. Phys. J. E, **39**, 125 (2016).

[5] A. Vailati and M. Giglio, Nature, **390**, 262 (1997).

664 [6] F. Croccolo, H. Bataller and F. Scheffold, J. Chem. Phys., **137**, 234202 (2012).
665 [7] C. Giraudet, H. Bataller and F. Croccolo, Eur. Phys. J. E, **37**, 107 (2014).
666 [8] C. Ludwig, Sitzungsbur. Osterr. Akad. Wiss., Math.-Nat. Kl., **20**, 539 (1856).
667 [9] C. Soret, Arch. Sci. Phys. Nat. Geneve, **2**, 48 (1879).
668 [10] W. Köhler and K. I. Morozov, J. Non-Equil. Thermody., **41**, 151 (2016).
669 [11] F. Croccolo and D. Brogioli, Appl. Optics, **50**, 3419 (2011).
670 [12] F. Croccolo, D. Brogioli, A. Vailati, M. Giglio and D. S. Cannell, Phys. Rev. E, **76**,
671 041112 (2007).
672 [13] S. P. Trainoff and D. S. Cannell, Phys. Fluids, **14**, 1340 (2002).
673 [14] H. Bataller, T. Triller, B. Pur, W. Köhler, J. M. Ortiz de Zarate and F. Croccolo, Eur.
674 Phys. J. E, **40**, 35 (2017).
675 [15] I. Lizarraga, C. Giraudet, F. Croccolo, M. M. Bou-Ali and H. Bataller, Microgravity Sci.
676 Tec., **28**, 545 (2016).
677 [16] J. K. Platten, M. M. Bou-Ali, P. Costesèque, J. F. Dutrieux, W. Köhler, C. Leppla, S.
678 Wiegand and G. Wittko, Philos. Mag., **83**, 1965 (2003).
679 [17] H. Bataller, C. Giraudet, F. Croccolo and J. M. Ortiz de Zárate, Microgravity Sci. Tec.,
680 **28**, 611 (2016).
681 [18] M. M. Bou-Ali, A. Ahadi, D. Alonso de Mezquia, Q. Galand, M. Gebhardt, O. Khlybov,
682 W. Köhler, M. Larranaga, J. C. Legros, T. Lyubimova, A. Mialdun, I. Ryzhkov, M. Z. Saghir,
683 V. Shevtsova and S. Van Vaerenbergh, Eur. Phys. J. E, **38**, 30 (2015).
684 [19] A. Ahadi, S. V. Varenbergh and M. Z. Saghir, J. Chem. Phys., **138**, 204201 (2013).
685 [20] A. Mialdun and V. Shevtsova, J. Chem. Phys., **143**, 224902 (2015).
686 [21] A. Mialdun, I. Ryzhkov, O. Khlybov, T. Lyubimova and V. Shevtsova, J. Chem. Phys.,
687 **148**, 044506 (2018).

[22] T. Triller, H. Bataller, M. M. Bou-Ali, M. Braibanti, F. Croccolo, J. M. Ezquerro, Q. Galand, J. Gavaldà, E. Lapeira, A. Laverón-Simavilla, T. Lyubimova, A. Mialdun, J. M. Ortiz de Zárate, J. Rodríguez, X. Ruiz, I. I. Ryzhkov, V. Shevtsova, S. V. Vaerenbergh and W. Köhler, Microgravity Sci. Tec., **30**, 295 (2018).

[23] A. Mialdun, H. Bataller, M. M. Bou-Ali, M. Braibanti, F. Croccolo, A. Errarte, J. M. Ezquerro, Y. Gaponenko, L. García-Fernández, J. J. Fernández, J. Rodríguez and V. Shevtsova, Eur. Phys. J. E, **42**, 87 (2019).

[24] G. Galliero, H. Bataller, J. P. Bazile, J. Diaz, F. Croccolo, H. Hoang, R. Vermorel, P. A. Artola, B. Rousseau, V. Vesovic, M. M. Bou-Ali, J. M. Ortiz de Zarate, S. Xu, K. Zhang, F. Montel, A. Verga and O. Minster, NPJ Microgravity, **3**, 20 (2017).

[25] J. C. Legros, V. Vaerenbergh, D. S., Y. and F. Montel, Entropy, **198/199**, 1 (1994).

[26] S. VanVaerenbergh, S. Srinivasan and M. Z. Saghir, J. Chem. Phys., **131**, 114505 (2009).

[27] G. Galliero, H. Bataller, F. Croccolo, R. Vermorel, P.-A. Artola, B. Rousseau, V. Vesovic, M. Bou-Ali, J. M. Ortiz de Zárate, S. Xu, K. Zhang and F. Montel, Microgravity Sci. Tec., **28**, 79 (2015).

[28] P. Baaske, H. Bataller, M. Braibanti, M. Carpineti, R. Cerbino, F. Croccolo, A. Donev, W. Köhler, J. M. Ortiz de Zarate and A. Vailati, Eur. Phys. J. E, **39**, 119 (2016).

[29] M. Braibanti, P.-A. Artola, P. Baaske, H. Bataller, J.-P. Bazile, M. M. Bou-Ali, D. S. Cannell, M. Carpineti, R. Cerbino, F. Croccolo, J. Diaz, A. Donev, A. Errarte, J. M. Ezquerro, Q. Galand, G. Galliero, Y. Gaponenko, L. García-Fernández, J. Gavaldá, F. Giavazzi, M. Giglio, H. Hoang, W. Köhler, E. Lapeira, A. Laverón-Simavilla, I. Lizarraga, T. Lyubimova, S. Mazzoni, A. Mialdun, O. Minster, F. Montel, J. M. O. d. Zárate, J. Rodríguez, B. Rousseau, X. Ruiz, I. I. Ryzhkov, M. Schraml, V. Shevtsova, C. J. Takacs, T. Triller, S. VanVaerenbergh, A. Vailati, A. Verga, R. Vermorel, V. Vesovic, V. Yasnou, S. Xu, D. Zapf and K. Zhang, Eur. Phys. J. E, **42**, 86 (2019).

[30] P. Blanco, M. M. Bou-Ali, J. K. Platten, D. A. de Mezquia, J. A. Madariaga and C. Santamaria, J. Chem. Phys., **132**, 114506 (2010).

[31] A. Leahy-Dios, M. M. Bou-Ali, J. K. Platten and A. Firoozabadi, J. Chem. Phys., **122**, 234502 (2005).

[32] A. Königer, H. Wunderlich and W. Köhler, J. Chem. Phys., **132**, 174506 (2010).

[33] A. Ahadi and M. Ziad Saghir, Eur. Phys. J. E, **38**, 25 (2015).

[34] A. Mialdun, J. C. Legros, V. Yasnou, V. Sechenyh and V. Shevtsova, Eur. Phys. J. E, **38**, 27 (2015).

[35] M. Gebhardt and W. Kohler, Eur. Phys. J. E, **38**, 24 (2015).

[36] Q. Galand and S. Van Vaerenbergh, Eur. Phys. J. E, **38**, 26 (2015).

[37] O. A. Khlybov, Ryzhkov, II and T. P. Lyubimova, Eur. Phys. J. E, **38**, 29 (2015).

[38] M. Larranaga, M. M. Bou-Ali, D. A. de Mezquia, D. A. Rees, J. A. Madariaga, C. Santamaria and J. K. Platten, Eur. Phys. J. E, **38**, 28 (2015).

[39] J. M. Ortiz de Zarate, C. Giraudet, H. Bataller and F. Croccolo, Eur. Phys. J. E, **37**, 77 (2014).

[40] P. Martínez Pancorbo, J. M. Ortiz de Zarate, H. Bataller and F. Croccolo, Eur. Phys. J. E, **40**, 22 (2017).

[41] C. Giraudet, H. Bataller, Y. Sun, A. Donev, J. M. Ortiz de Zárate and F. Croccolo, EPL-Europhys. Lett., **111**, 60013 (2015).

[42] C. Giraudet, H. Bataller, Y. Sun, A. Donev, J. M. Ortiz de Zarate and F. Croccolo, Eur. Phys. J. E, **39**, 120 (2016).

[43] F. Croccolo, L. García-Fernández, H. Bataller, A. Vailati and J. M. Ortiz de Zarate, Phys. Rev. E, **99**, 012602 (2019).

[44] D. Alonso de Mezquia, Z. Wang, E. Lapeira, M. Klein, S. Wiegand and M. Mounir Bou-Ali, Eur. Phys. J. E, **37**, 106 (2014).

[45] J. Rauch and W. Köhler, J. Chem. Phys., **119**, 11977 (2003).

[46] K. J. Zhang, M. E. Briggs, R. W. Gammon and J. V. Sengers, J. Chem. Phys., **104**, 6881 (1996).

[47] D. Brogioli, A. Vailati and M. Giglio, Phys. Rev. E, **61**, 1 (2000).

[48] F. Croccolo, D. Brogioli, A. Vailati, M. Giglio and D. S. Cannell, Appl. Optics, **45**, 2166 (2006).

[49] G. Cerchiari, F. Croccolo, F. Cardinaux and F. Scheffold, Rev. Sci. Instrum., **83**, 106101 (2012).

[50] L. Cipelletti and D. A. Weitz, Rev. Sci. Instrum., **70**, 3214 (1999).

[51] J. M. Ortiz de Zarate, Eur. Phys. J. E, **42**, 43 (2019).

[52] J. M. Ortiz de Zárate, J. L. Hita and J. V. Sengers, CR. Mecanique, **341**, 399 (2013).

[53] A. Bardow, Fluid Phase Equilibria, **251**, 121 (2007).

[54] P. N. Segrè, R. Schmitz and J. V. Sengers, Physica A, **195**, 31 (1993).

[55] F. Croccolo, C. Giraudet, H. Bataller, R. Cerbino and A. Vailati, Microgravity Sci. Tec., **28**, 467 (2016).